Acta Mech 227, 3261–3273 (2016)
DOI 10.1007/s00707-015-1542-9

ORIGINAL PAPER

Marco Antonio Meggiolaro · Jaime Tupiassú Pinho de Castro · Hao Wu

Generalization of the moment of inertia method to estimate equivalent amplitudes for simplifying the analysis of arbitrary non-proportional multiaxial stress or strain histories

Received: 31 December 2014 / Revised: 22 July 2015 / Published online: 16 January 2016

Abstract Several models have been proposed in the literature to account for fatigue damage under multiaxial load histories. Most of them require some measure of an equivalent stress or strain amplitude, in the sense of causing the same damage as the original history, which may be difficult to obtain for generic non-proportional multiaxial variable amplitude load histories. To identify individual load cycles, a multiaxial rainflow-like algorithm must be employed. For each rainflow-counted cycle, the equivalent stress or strain amplitude along its path is often computed using the so-called convex enclosure methods, which find minimum spheres, ellipsoids, or rectangular prisms that contain the load path in a deviatoric stress or strain space. However, such procedure involves information loss, in special if the path shape is very different from the shape of the enclosing convex surface, resulting in poor estimates of equivalent stress or strain amplitudes. To overcome this problem, the moment of inertia (MOI) method has been proposed in Meggiolaro and Castro (Int J Fatigue 42:217–226, 2012) to calculate equivalent amplitudes and mean components of two-dimensional stress or strain paths, generated, e.g., by tension–torsion or biaxial histories. In this work, the MOI method is extended to deal with generic 6D stress or strain paths, which include all normal and shear components. To accomplish that, the load history path is first represented in a 5D deviatoric stress or strain space and then assumed to be a homogeneous wire with unit mass, whose perimeter centroid is used to estimate the location of the path mean component. Then, the polar moment of inertia (PMOI) of such a hypothetical wire with respect to its mean component is calculated. The PMOI represents the distribution of the path about a single point, the perimeter centroid, giving a measure of how much the path stretches away from its mean component, which is used in the calculation of the equivalent amplitudes. Experimental results for 13 different multiaxial load histories prove the effectiveness of the proposed method to predict equivalent amplitudes and multiaxial fatigue lives.

1 Introduction

Service loads can act on only one or on several points of a structural component, and they can be generated by a single or by multiple sources, coherent or not. In general, such loads can cause bending, torsion, normal, and/or

M. A. Meggiolaro (✉) · J. T. P. de Castro
Pontifical Catholic University of Rio de Janeiro, PUC-Rio, Rua Marquês de São Vicente 225,
Rio de Janeiro, RJ 22451-900, Brazil
E-mail: meggi@puc-rio.br

J. T. P. de Castro
E-mail: jtcastro@puc-rio.br

H. Wu
School of Aerospace Engineering and Applied Mechanics, Tongji University, Siping Road 1239, Shanghai 200092,
People's Republic of China
E-mail: wuhao@tongji.edu.cn

shear efforts, which when combined can induce multiaxial stress histories at critical points of the component. Multiaxial fatigue deals with the initiation and/or the propagation of fatigue cracks under such general conditions. Multiaxial fatigue load histories can be proportional or non-proportional. They are proportional when the principal axes of the stresses and strains induced by them at the critical point, and thus their associated maximum-shear planes remain fixed during their entire duration. On the other hand, non-proportional (NP) loads induce principal stress/strain directions that change in time.

Consider for instance a tension–torsion problem where a shaft is loaded by a normal stress $\sigma_x(t)$ in the x direction combined with a shear stress $\tau_{xy}(t)$, where t stands for time. When the shear and normal stresses are directly proportional, the ratio $\tau_{xy}(t)/\sigma_x(t)$ and the angle between σ_1 and the x axis $\theta_1(t) = 0.5 \cdot \tan^{-1}[2\tau_{xy}(t)/\sigma_x(t)]$ remain fixed for all t, and thus this simple multiaxial load history is proportional. If $\tau_{xy}(t)/\sigma_x(t)$ and so $\theta_1(t)$ as well vary with time, then the loading is NP. The relative degree of non-proportionality is quantified by the non-proportionality factor F_{NP}, which ranges from zero (for a proportional history) to one (for a fully NP history). If all stress and strain components are periodic and have the same frequency, they can also be classified as in-phase or out-of-phase. Both the in-phase and 180° out-of-phase loadings usually have a fixed $\tau_{xy}(t)/\sigma_x(t)$ ratio and induce proportional histories with $F_{\mathrm{NP}} = 0$, unless they do not cross the $\sigma_x \times \tau_{xy}\sqrt{3}$ plane origin, when they are NP because they then have a variable $\tau_{xy}(t)/\sigma_x(t)$ ratio. The 90° out-of-phase loading, on the other hand, always results in an NP history, with F_{NP} depending on the ratio between the shear and normal amplitudes. Experimental evidence in tension–torsion histories indicates that the maximum $F_{\mathrm{NP}} = 1$ value is achieved when the von Mises stress $\sqrt{\sigma_x^2 + 3\tau_{xy}^2}$ is fixed along the load path, e.g., for sinusoidal 90° out-of-phase loadings with equal amplitudes for σ_x and $\tau_{xy}\sqrt{3}$.

Materials can be divided into two main classes regarding their multiaxial fatigue damage mechanism, namely directional- and distributed-damage materials. Directional-damage materials, like most metals, fail by fatigue due to a single dominant crack in a so-called the critical plane, whose direction must be determined using damage models that take into account the stress and strain histories projected onto it. For such materials, it is usual to neglect fatigue damage eventually induced on other planes, assuming that it does not interact nor affect the crack initiation process on the critical plane and thus that multiaxial fatigue damage can be calculated based only on the normal and shear stress (and/or strain) histories acting on the critical plane. The search for the critical plane direction can be performed using the critical-damage approach, see, e.g., [2] for details.

Distributed-damage materials, on the other hand, fail by multiaxial fatigue due to distributed mechanisms, which may cause, e.g., multiple cracking in concrete or cavitation in ductile metals under high loads. Fiber-reinforced composites fail by distributed mechanisms as well, because fiber rupture happens along their multiple directions, so they usually need to be described by anisotropic damage models. Moreover, even though multiple cracks in concrete and fiber rupture in composites can happen in several different directions, all of them can contribute altogether to the accumulated damage in such materials, and in addition to the decrease or loss of their stiffness. Consequently, there is a significant interaction among damage mechanisms acting on different planes or directions in distributed-damage materials, as opposed to what happens in directional-damage materials. Fatigue calculations in distributed-damage materials usually involve some invariant like the von Mises equivalent stress or strain and the hydrostatic component, which can mix stress and/or strain contributions in all directions into the calculation of multiaxial damage, without assuming a preferential plane. Alternatively to invariant-based approaches, models based on continuum damage mechanics principles explore the material stiffness loss caused, e.g., by multiple cracks or voids to try to predict fatigue damage accumulation induced by variable uniaxial or multiaxial loads.

Multiaxial fatigue predictions are not trivial problems. On the contrary, they can even become quite challenging for general NP load histories, particularly when they induce elastoplastic (EP) stresses and strains, due to at least 5 potential issues involving:

1. Stress–strain relationships: Uniaxial stress–strain curves such as Ramberg–Osgood cannot be directly applied to multiaxial problems. Approximate models have been proposed to calculate the relations between the 6 stress and 6 strain components induced by proportional load histories. However, a much more complex approach involving suitable incremental plasticity algorithms is required for proper modeling NP histories, and in such cases the stress–strain solution must be obtained from the integration of a set of differential equations;
2. NP strain hardening: Some materials can strain-harden much more than it would be expected from the uniaxial cyclic $\sigma\varepsilon$ curve when subjected non-proportional (NP) multiaxial cyclic loads. This phenomenon,

called NP hardening, cross-hardening, or additional (NP) strain hardening, depends on the load history, through the NP factor, and on the material, through the additional hardening coefficient $0 \leq \alpha_{\mathrm{NP}} \leq 1$. NP hardening is usually modeled using the same exponent h_c from the uniaxial cyclic Ramberg–Osgood curve, assuming that it does not vary while the hardening coefficient is gradually increased from H_c to H_{NP}, and the NP hardening coefficient associated with NP multiaxial loads $H_{\mathrm{NP}} = H_c \cdot (1 + \alpha_{\mathrm{NP}} \cdot F_{\mathrm{NP}})$. Under NP loads, the ratio $\Delta\sigma/\Delta\varepsilon$ between the stress and strain ranges in such materials gradually increases at every cycle, a phenomenon called NP hardening or additional hardening. This effect can significantly decrease the fatigue life of components subjected to strain-controlled load histories;

3. *Damage calculation*: Traditional SN and εN curves, measured under proportional loading, cannot be directly employed in NP histories, because the variation of the principal directions may change the crack initiation plane and, therefore, the associated fatigue lives;
4. *Cycle counting*: The traditional rainflow counting techniques cannot be applied to variable amplitude NP loadings, because the peaks and valleys of each stress or strain component in general do not coincide with the peaks and valleys of the other components, becoming impossible to decide a priori which points should be considered as load reversions; and
5. *Stress and strain concentration factors*: K_σ and K_ε are equal under uniaxial linear elastic (LE) loads in plane stress (pl-σ), but usually $K_\sigma \neq K_\varepsilon$ under multiaxial loads, even if LE and pl-σ. Moreover, even uniaxial nominal loads can induce multiaxial NP histories at notch tips in the EP case, due to triaxial stresses around them and to the difference between the elastic and plastic Poisson ratios (the elastic Poisson ratios for metals, typically within $1/4 \leq \nu_{\mathrm{el}} = \nu \leq 1/3$, are significantly smaller than their plastic Poisson ratio $\nu_{\mathrm{pl}} = 0.5$, since plastic strains conserve volume while they cause no cavitation.)

This work addresses some practical problems related to issues 1 and 2, since the proper identification of equivalent stress or strain ranges and peaks within a generic NP load history is a necessary step for applying most multiaxial fatigue damage models. Indeed, they are the main driving force for crack initiation, a process that depends on the stress range and usually is affected by the peak or mean components as well [1]. Moreover, these equivalent ranges must take into account the shape of the load history in a stress or strain diagram (like the $\sigma_x \times \tau_{xy}\sqrt{3}$ plane for tension–torsion loads), since it can much affect fatigue damage under multiaxial loads. Indeed, it is well known that a circular out-of-phase tension–torsion load path may have a much more damaging effect than a proportional straight tension–torsion path with the same extreme values [2]. However, generic multiaxial loading conditions, which in each load event may involve variations of 6 stress or strain components, are not that easy to deal with in practical applications. The objective of this work is to propose a model that can be efficiently applied to estimate equivalent amplitude and mean stress or strain components in such cases and that can be relatively easy implemented in suitable computer codes.

To do so, first the 6D applied stress or strain history must be represented in a much more efficient transformed 5D deviatoric stress space E_{5s} (for stress histories) or strain space E_{5e} (for strain histories). These 5D deviatoric spaces represent the stress and strain states using the 5D vectors $\vec{s}'$ and $\vec{e}'$, defined as

$$\begin{cases} \vec{s}' \equiv [\, s_1 \; s_2 \; s_3 \; s_4 \; s_5 \,]^T \quad \text{and} \quad \vec{e}' \equiv [\, e_1 \; e_2 \; e_3 \; e_4 \; e_5 \,]^T \\ s_1 \equiv \sigma_x - \frac{\sigma_y+\sigma_z}{2}, \quad s_2 \equiv \frac{\sigma_y-\sigma_z}{2}\sqrt{3}, \quad s_3 \equiv \tau_{xy}\sqrt{3}, \quad s_4 \equiv \tau_{xz}\sqrt{3}, \quad s_5 \equiv \tau_{yz}\sqrt{3} \\ e_1 \equiv \varepsilon_x - \frac{\varepsilon_y+\varepsilon_z}{2}, \quad e_2 \equiv \frac{\varepsilon_y-\varepsilon_z}{2}\sqrt{3}, \quad e_3 \equiv \frac{\gamma_{xy}}{2}\sqrt{3}, \quad e_4 \equiv \frac{\gamma_{xz}}{2}\sqrt{3}, \quad e_5 \equiv \frac{\gamma_{yz}}{2}\sqrt{3} \end{cases} \tag{1}$$

Such deviatoric spaces are advantageous over the original 6D stress or strain spaces needed to describe generic multiaxial loads because their Euclidean stress and strain norms $|\vec{s}'|$ and $|\vec{e}'|/(1+\bar{\nu})$ are equal to the von Mises equivalent stresses and strains σ_{Mises} and $\varepsilon_{\mathrm{Mises}}$, where $\bar{\nu}$ is a so-called effective elastoplastic Poisson ratio that considers the contribution of the elastic and plastic stress or strain components, which are associated to ratios ν_{el} and to 0.5, respectively.

Several convex enclosure methods have been proposed to calculate equivalent stress or strain ranges and mean loads using deviatoric sub-spaces similar to the ones defined in Eq. (1) [3–12]. However, their shortcomings become evident when they are applied to more complex non-convex multiaxial load history paths, as explained in detail in [1]. To overcome most of those shortcomings and thus better estimate these equivalent ranges and means for general multiaxial NP histories, the MOI method has been proposed in [1], originally in its 2D formulation.

In the MOI method, the stress or strain path in the 5D deviatoric spaces is assumed to be analogous to a homogeneous wire with unit mass, whose center of mass (centroid) is used to estimate the location of the mean component of the load path. Then, the polar moment of inertia (PMOI) of such hypothetical wire with respect

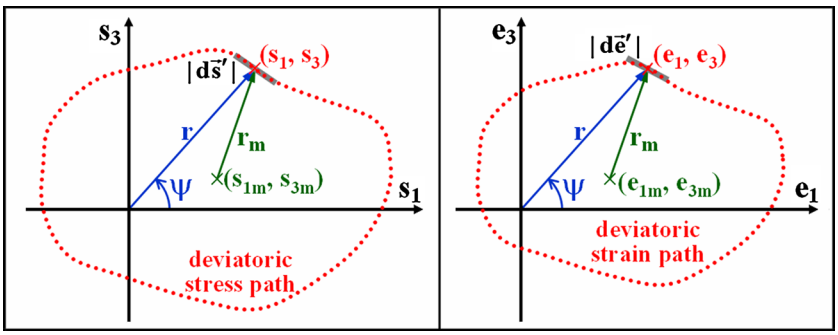

Fig. 1 Stress path of a 2D tension–torsion load history in the deviatoric $s_1 \times s_3$ diagram (*left*) and its corresponding strain path in the $e_1 \times e_3$ diagram (*right*), both assumed as homogeneous wires with unit mass

to its centroid is calculated, which gives a measure of how much the load path stretches away from its mean component. The path-equivalent range of the true stress or strain path is finally calculated as a function of this PMOI, which is a physically sound approximation, since paths with larger amplitudes would be associated with wider wires with increased PMOI. The original 2D version of the MOI method is detailed next, and then it is extended to deal with generic 6D multiaxial loading conditions in the following sections.

2 The MOI method for 2D multiaxial load histories

Before generalizing the MOI method to deal with generic 6D multiaxial loading histories, lets formulate it to calculate the equivalent range and mean components of simpler elastoplastic tension–torsion 2D histories with stress paths that can be defined by the normal and shear components σ_x and τ_{xy}. Since in such cases $\sigma_y = \sigma_z = \tau_{xz} = \tau_{yz} = 0$, while $\gamma_{xz} = \gamma_{yz} = 0$ and $\varepsilon_y = \varepsilon_z = -\bar{\nu} \cdot \varepsilon_x$, it follows that

$$s_1 \equiv \sigma_x, \quad s_2 \equiv 0, \quad s_3 \equiv \tau_{xy}\sqrt{3}, \quad s_4 \equiv 0, \quad s_5 \equiv 0, \tag{2}$$

$$e_1 \equiv \varepsilon_x - \frac{\varepsilon_y + \varepsilon_z}{2} = \varepsilon_x \cdot (1 + \bar{\nu}), \quad e_2 \equiv \frac{\varepsilon_y - \varepsilon_z}{2}\sqrt{3} = 0, \quad e_3 \equiv \frac{\gamma_{xy}}{2}\sqrt{3}, \quad e_4 = e_5 \equiv 0. \tag{3}$$

Since only s_1, s_3, e_1, and e_3 are different from zero, the stress or strain paths of such tension–torsion histories can be represented in 2D deviatoric stress or strain diagrams $s_1 \times s_3 \equiv \sigma_x \times \tau_{xy}\sqrt{3}$ or $e_1 \times e_3 = [\varepsilon_x \cdot (1 + \bar{\nu}) \times \gamma_{xy}\sqrt{3}/2]$, as shown in Fig. 1.

The MOI method assumes that such 2D load paths, which are represented by a series of points (s_1, s_3) or (e_1, e_3) that describe the deviatoric stress or strain variations along it, are analogous to a homogeneous wire with unit mass. The mean component of the path is assumed to be located at the center of gravity of this hypothetical homogeneous wire shaped as the load history path. This center of gravity is located at the perimeter centroid (s_{1m}, s_{3m}) or (e_{1m}, e_{3m}) of the stress or strain paths, calculated from its contour integrals

$$s_{1m} = (1/p_s) \cdot \int s_1 \cdot |\mathrm{d}\vec{s}'|, \quad s_{3m} = (1/p_s) \cdot \int s_3 \cdot |\mathrm{d}\vec{s}'|, \quad p_s = \int |\mathrm{d}\vec{s}'|, \tag{4}$$

$$e_{1m} = (1/p_e) \cdot \int e_1 \cdot |\mathrm{d}\vec{e}'|, \quad e_{3m} = (1/p_e) \cdot \int e_3 \cdot |\mathrm{d}\vec{e}'|, \quad p_e = \int |\mathrm{d}\vec{e}'|, \tag{5}$$

where $|\mathrm{d}\vec{s}'|$ and $|\mathrm{d}\vec{e}'|$ are the lengths of infinitesimal segments of the stress and strain paths, while p_s and p_e are the respective path perimeters, see Fig. 1.

Note that the perimeter centroid is in general different from the area centroid, which would be the center of gravity of a uniform density sheet bounded by the shape of the closed load path. The reason to choose the perimeter centroid instead of the area centroid to locate the mean component of the load paths can be readily seen in the simple example illustrated in Fig. 2.

In this example, note that the right portion of the stress or strain history has almost zero area, and hence it allows the area centroid AC to be located approximately at the origin of the diagram, which is not a physically reasonable analogy for the mean load associated with such an asymmetrical load path. The perimeter centroid

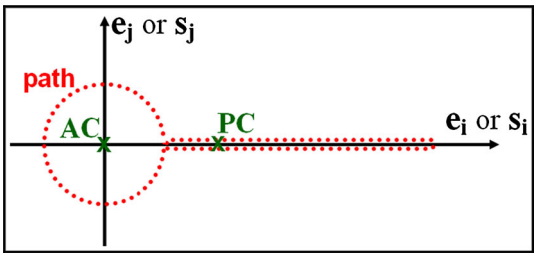

Fig. 2 Stress or strain path represented in the deviatoric sub-space $s_i \times s_j$ or $e_i \times e_j$ of the E_{5s} and E_{5e} spaces (with $1 \leq i < j \leq 5$), whose positive mean component is much better estimated from the perimeter centroid (PC) than from the area centroid (AC)

PC, on the other hand, gives a much more reasonable estimate of the mean component of such stress or strain path.

Note, however, that (s_{1m}, s_{3m}) and (e_{1m}, e_{3m}) are the mean components of *deviatoric* stress or strain paths, so to compute the actual mean stresses and strains it is necessary to include the contribution of the mean hydrostatic stress σ_{hm} and strain ε_{hm} components, obtained after averaging the hydrostatic σ_h and ε_h along the original history through

$$\sigma_{hm} = (1/p_s) \cdot \int \sigma_h \cdot |\mathrm{d}\vec{s}'| \quad \text{and} \quad \varepsilon_{hm} = (1/p_e) \cdot \int \varepsilon_h \cdot |\mathrm{d}\vec{e}'|. \tag{6}$$

Since the tension–torsion history has hydrostatic components $\sigma_h = \sigma_x/3 = s_1/3$ (so $\sigma_{hm} = s_{1m}/3$) and $\varepsilon_h = (\varepsilon_x + \varepsilon_y + \varepsilon_z)/3 = \varepsilon_x \cdot (1 - 2\bar{\nu})/3$ (so $\varepsilon_{hm} = \varepsilon_{xm} \cdot (1 - 2\bar{\nu})/3$), and deviatoric components $s_2 = s_4 = s_5 = 0$ and $e_2 = e_4 = e_5 = 0$, it can be shown that

$$\begin{cases} \sigma_{xm} = \sigma_{hm} + s_{1m} \cdot 2/3 = s_{1m} \\ \sigma_{ym} = \sigma_{zm} = \sigma_{hm} - s_{1m}/3 = 0 \\ \tau_{xym} = s_{3m}/\sqrt{3},\ \tau_{xzm} = \tau_{yzm} = 0 \end{cases} \quad \text{and} \quad \begin{cases} \varepsilon_{xm} = \varepsilon_{hm} + e_{1m} \cdot 2/3 = e_{1m}/(1 + \bar{\nu}) \\ \varepsilon_{ym} = \varepsilon_{zm} = \varepsilon_{hm} - e_{1m}/3 = -\bar{\nu} \cdot \varepsilon_{xm} \\ \gamma_{xym} = e_{3m} \cdot 2/\sqrt{3},\ \gamma_{xzm} = \gamma_{yzm} = 0 \end{cases} \tag{7}$$

As stated above, the MOI method calculates the equivalent range of a stress or strain path from the mass moment of inertia (MOI) of a corresponding homogeneous wire with unit mass. But instead of using the Axial MOI (AMOI) of the wire, which is calculated about a given *axis*, the Polar MOI (PMOI) is adopted instead, since it represents the distribution of the load path about a *single point*, its perimeter centroid. The PMOI of the stress or strain path about the perimeter centroid is then obtained from the contour integral of the square of the distance r_m between each point in the path and the path centroid (see Fig. 1), resulting in

$$I_p \equiv \frac{1}{p_s} \cdot \int \underbrace{\left[(s_1 - s_{1m})^2 + (s_3 - s_{3m})^2\right]}_{{r_m}^2} \cdot |\mathrm{d}\vec{s}'| \quad \text{or} \quad \frac{1}{p_e} \cdot \int \underbrace{\left[(e_1 - e_{1m})^2 + (e_3 - e_{3m})^2\right]}_{{r_m}^2} \cdot |\mathrm{d}\vec{e}'|. \tag{8}$$

The path-equivalent ranges are assumed proportional to the radius of gyration of the path, which is equal to the square root of the unit mass wire PMOI. This hypothesis is physically sound, since load history path segments that are further away from its mean component contribute more to the path-equivalent range, in the same way that the analogous wire segments further away from the path perimeter centroid contribute more to the PMOI of its imaginary homogeneous wire. The path-equivalent stress and strain ranges become then

$$\Delta\sigma_{\text{Mises}} \text{ or } \Delta\varepsilon_{\text{Mises}} \cdot (1 + \bar{\nu}) = \sqrt{12 \cdot I_p}. \tag{9}$$

Note that the $\sqrt{12}$ factor has been introduced in this equation to guarantee that a proportional loading path, represented by two straight segments with length L and unit mass $m = 1$ (see Fig. 3), will result in the expected range $\Delta\sigma_{\text{Mises}}$ or $\Delta\varepsilon_{\text{Mises}} \cdot (1 + \bar{\nu})$ equal to L,

$$I_p = m \cdot L^2/12 \Rightarrow \Delta\sigma_{\text{Mises}} \text{ or } \Delta\varepsilon_{\text{Mises}} \cdot (1 + \bar{\nu}) = \sqrt{12 \cdot 1 \cdot L^2/12} = L, \tag{10}$$

since the MOI of a straight wire with respect to its centroid is $m \cdot L^2/12$, and $m = 1$ (because the wire that represents the load path is assumed to have a unit mass).

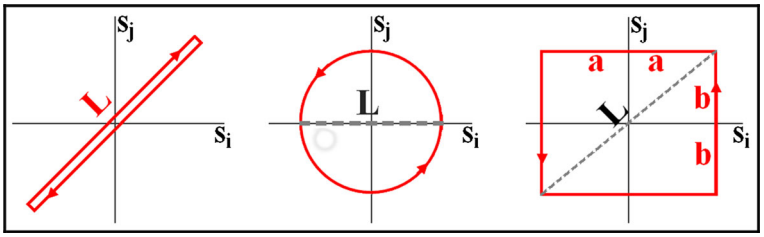

Fig. 3 Proportional, circular, and rectangular stress paths showing a full loading cycle

For a circular load path with diameter L (see Fig. 3), I_p is obtained from the PMOI of a unit mass ring,

$$I_p = m \cdot (L/2)^2 \Rightarrow \Delta\sigma_{\text{Mises}} \text{ or } \Delta\varepsilon_{\text{Mises}} \cdot (1+\bar{\nu}) = \sqrt{12 \cdot \left(1 \cdot L^2/4\right)} = L\sqrt{3}. \tag{11}$$

Note that this result differs from the estimates of most convex enclosure methods [3–12], which would predict $L\sqrt{2}$ for the path-equivalent von Mises range in this case. But the higher $L\sqrt{3}$ range predicted by the MOI method is physically more reasonable. Indeed, a square path with diagonal L (which is its longest chord) also has a path-equivalent von Mises range $L\sqrt{2}$ according to most convex enclosure methods. However, it is reasonable to assume that a circular path circumscribing such square, which would describe a 57 % larger area in the load diagram, should result in a somewhat larger path-equivalent stress or strain range, e.g., 22.5 % larger as predicted by the MOI method.

In fact, experiments with both circular and square multiaxial load paths with same longest chord L result in significantly different fatigue lives, a difference that most convex enclosure methods are not able to predict. Hence, the $L\sqrt{3}$ MOI prediction for the von Mises range of circular load paths can be claimed to be better than the $L\sqrt{2}$ estimate obtained from convex enclosure methods.

To further exemplify the MOI method, lets now calculate the path-equivalent von Mises range for a rectangular path with sides $2a$ and $2b$ centered at the origin, as shown in Fig. 3, setting $i = 1$ and $j = 3$ to represent a tension–torsion problem. Imagining such path as a homogeneous wire with unit mass, then its perimeter in the deviatoric stress space $s_1 \times s_3$ is $p_s = 4a + 4b$. Each of the two horizontal path segments is modeled as a rod with mass $m_a = 2a/p_s$, while each vertical segment is a rod with $m_b = 2b/p_s$, so that the sum of the masses of all four rods is $2 \cdot m_a + 2 \cdot m_b = 2 \cdot (2a + 2b)/p_s = 1$, the unit mass condition required by the MOI method. The longest chord of the path is the diagonal of the rectangular path, $L = 2 \cdot (a^2 + b^2)^{1/2}$. From the loading path symmetry, the perimeter centroid (s_{1m}, s_{3m}) is located at the origin, and therefore, the PMOI I_p is the sum of the PMOI contributions of the four rods with respect to the origin. From the *parallel axis theorem* [13], it follows that

$$I_p = 2 \cdot \underbrace{(m_a a^2/3 + m_a b^2)}_{\text{horizontal rods}} + 2 \cdot \underbrace{(m_b b^2/3 + m_b a^2)}_{\text{vertical rods}} = \frac{(2a+2b)^3}{6 \cdot p_s} = \frac{(2a+2b)^2}{12} \tag{12}$$

and therefore

$$\Delta\sigma_{\text{Mises}} = \sqrt{12 \cdot (2a+2b)^2/12} = 2 \cdot (a+b), \tag{13}$$

which is exactly the value predicted by the Maximum Prismatic Hull method [8], resulting in a ratio

$$\lambda_{\text{MOI}} \equiv \Delta\sigma_{\text{Mises}}/L = (a+b)/\sqrt{a^2+b^2}. \tag{14}$$

Note that the MOI estimates for the path-equivalent range are independent of the choice of the coordinate system, since the path PMOI about its centroid depends only on its shape. So, the $\Delta\sigma_{\text{Mises}}$ of any rectangular path with sides $2a$ and $2b$ estimated by the MOI method is always $2 \cdot (a+b)$, even if it is rotated or its centroid is not located at the origin of the diagram. The possibility of using the traditional properties of mass moments of inertia to get hints about the behavior of multiaxial load histories is certainly an additional advantage of the MOI method.

Moreover, from a practical point of view the MOI estimates for the von Mises range are quite simple to calculate, especially for polygonal load histories. The moments of curved paths are also easy to calculate from fine polygonal discretizations. In addition, the MOI method can make use of classical mass MOI tables or even CAD programs that can be applied to arbitrarily shaped homogeneous wires to calculate I_p.

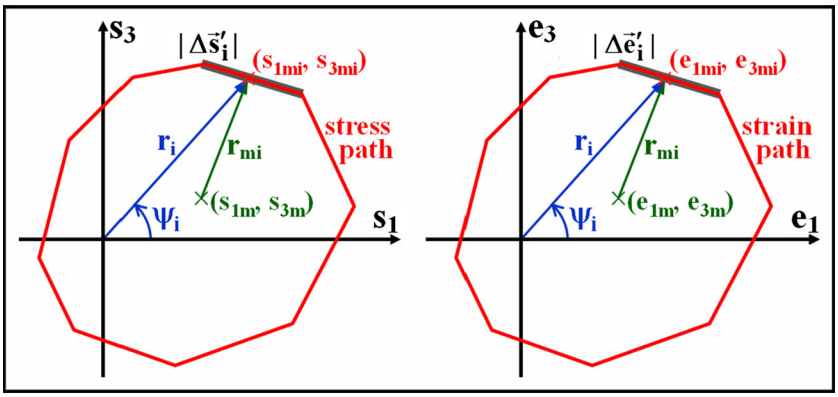

Fig. 4 Polygonal stress and strain paths in the $s_1 \times s_3$ and $e_1 \times e_3$ diagrams

To estimate von Mises ranges for polygonal multiaxial load paths by the MOI method, it is enough to combine the PMOI of a straight wire segment with the parallel axis theorem. For instance, for a polygonal stress path in the $s_1 \times s_3$ diagram, composed by straight segments with length $|\Delta\vec{s}'_i|$ centered at (s_{1mi}, s_{3mi}), as shown in Fig. 4, the perimeter centroid (s_{1m}, s_{3m}) and its PMOI I_p for a full loading cycle are obtained in a discrete formulation from the summations

$$\begin{aligned} p_s &= \sum_i |\Delta\vec{s}'_i|, \quad s_{1m} = (1/p_s) \cdot \sum_i s_{1mi} \cdot |\Delta\vec{s}'_i|, \quad s_{3m} = (1/p_s) \cdot \sum_i s_{3mi} \cdot |\Delta\vec{s}'_i|, \\ I_p &= (1/p_s) \cdot \sum_i [|\Delta\vec{s}'_i|^2/12 + \underbrace{(s_{1mi} - s_{1m})^2 + (s_{3mi} - s_{3m})^2}_{r_{mi}{}^2}] \cdot |\Delta\vec{s}'_i|. \end{aligned} \tag{15}$$

Analogously, for a polygonal multiaxial strain path with side lengths $|\Delta\vec{e}'_i|$ centered at the point (e_{1mi}, e_{3mi}), as shown in Fig. 4, the perimeter centroid (e_{1m}, e_{3m}) and its PMOI I_p for a full loading cycle become

$$\begin{aligned} p_e &= \sum_i |\Delta\vec{e}'_i|, \quad e_{1m} = (1/p_e) \cdot \sum_i e_{1mi} \cdot |\Delta\vec{e}'_i|, \quad e_{3m} = (1/p_e) \cdot \sum_i e_{3mi} \cdot |\Delta\vec{e}'_i|, \\ I_p &= (1/p_e) \cdot \sum_i [|\Delta\vec{e}'_i|^2/12 + \underbrace{(e_{1mi} - e_{1m})^2 + (e_{3mi} - e_{3m})^2}_{r_{mi}{}^2}] \cdot |\Delta\vec{e}'_i|. \end{aligned} \tag{16}$$

The path-equivalent von Mises stress and strain ranges can be then calculated from Eq. (9), and the mean hydrostatic stress σ_{hm} and strain ε_{hm} are estimated from the mean hydrostatic components σ_{hmi} and strain ε_{hmi} from each load segment i, using

$$\sigma_{hm} = (1/p_s) \cdot \sum_i \sigma_{hmi} \cdot |\Delta\vec{s}'_i| \quad \text{and} \quad \varepsilon_{hm} = (1/p_e) \cdot \sum_i \varepsilon_{hmi} \cdot |\Delta\vec{e}'_i|. \tag{17}$$

3 The MOI method for general 6D multiaxial load histories

In this section, the MOI method is generalized from its original 2D version to estimate the alternate and mean components of any general multiaxial load path involving all six stress or strain components.

To start with, it is important to recall that the critical plane approaches, those needed to describe multiaxial fatigue damage in most metallic alloys [14,15], require at most the calculation of the alternate and mean components of a 2D shear stress or strain path, for mixed Mode II–III shear cracks that initiate at 45° from a free surface, where the two shear stress or strain histories acting on the candidate plane should be combined to find equivalent shear ranges. Thus, for the critical plane approach, only the 2D version of the MOI method is required, applicable for materials that fail due to a single dominant crack.

But for materials that fail due to distributed damage, it is recommended to adopt a damage model based on an invariant such as von Mises, requiring a 6D (and thus a 5D deviatoric) formulation. Therefore, multiaxial fatigue damage models based on stress or strain invariants, such as Sines [16] and Crossland [17], need to find the alternate and mean components of a general 6D stress or strain path under general NP loading conditions, without any projection onto candidate planes, thus justifying the need to generalize the MOI method.

Note that the original versions of the Sines and Crossland models include very primitive definitions of equivalent ranges, which are only appropriate for very simple convex stress paths. To deal with more complex stress (or strain) paths, improved invariant-based models have been proposed in the literature, such as Papadopoulos' [18] and Papuga's [19] invariant-based models, which require the calculation of Novozhilov integrals [20] to find out the equivalent ranges and damage parameters. Instead of requiring the calculation of these computer-intensive integrals, the 6D MOI method could be used instead to find the equivalent ranges and then applied to improved versions of Sines' and Crossland's models or other invariant-based methods.

When a 6D stress or strain path is represented in the 5D sub-space associated with $\vec{s}'$ or $\vec{e}'$, the stress or strain scalar quantities associated with its PMOI can be defined as

$$I_p \equiv (1/p_s)\cdot\int \underbrace{|\vec{s}'-\vec{s}'_m|^2}_{r_m}\cdot|\mathrm{d}\vec{s}'| \quad \text{or} \quad I_p \equiv (1/p_e)\cdot\int \underbrace{|\vec{e}'-\vec{e}'_m|^2}_{r_m}\cdot|\mathrm{d}\vec{e}'|, \tag{18}$$

where $|\mathrm{d}\vec{s}'|$ and $|\mathrm{d}\vec{e}'|$ are the lengths of infinitesimal segments of the stress and strain paths, p_s and p_e are the respective path perimeters, r_m is the distance between each point in the path and its centroid, and the mean component $\vec{s}'_m$ or $\vec{e}'_m$ of the deviatoric path (located at its perimeter centroid) is given by

$$\vec{s}'_m = (1/p_s)\cdot\int \vec{s}'\cdot|\mathrm{d}\vec{s}'|, \quad p_s \equiv \int|\mathrm{d}\vec{s}'| \quad \text{or} \quad \vec{e}'_m = (1/p_e)\cdot\int \vec{e}'\cdot|\mathrm{d}\vec{e}'|, \quad p_e \equiv \int|\mathrm{d}\vec{e}'|. \tag{19}$$

Once again, to compute the actual mean stresses and strains, it is necessary to include the contribution of the mean hydrostatic stress σ_{hm} and strain ε_{hm} calculated in Eq. (6). The actual mean stress and strain components in the 6D Voigt–Mandel vectorial representation [21] become

$$\vec{\sigma}_m = (2/3)\cdot A^T\cdot\vec{s}'_m + \vec{\sigma}_{hm} \quad \text{and} \quad \vec{\varepsilon}_m = (2/3)\cdot A^T\cdot\vec{e}'_m + \vec{\varepsilon}_{hm}, \tag{20}$$

where T stands for the transpose of a matrix, the transformation matrix A between the 5D and Voigt–Mandel's 6D representation is

$$\vec{s}' = \begin{bmatrix} s_1\\ s_2\\ s_3\\ s_4\\ s_5 \end{bmatrix} = \underbrace{\begin{bmatrix} 1 & -1/2 & -1/2 & 0 & 0 & 0\\ 0 & \sqrt{3}/2 & -\sqrt{3}/2 & 0 & 0 & 0\\ 0 & 0 & 0 & \sqrt{3/2} & 0 & 0\\ 0 & 0 & 0 & 0 & \sqrt{3/2} & 0\\ 0 & 0 & 0 & 0 & 0 & \sqrt{3/2} \end{bmatrix}}_{A} \cdot \begin{bmatrix} \sigma_x\\ \sigma_y\\ \sigma_z\\ \tau_{xy}\sqrt{2}\\ \tau_{xz}\sqrt{2}\\ \tau_{yz}\sqrt{2} \end{bmatrix} = A\cdot\vec{\sigma}, \tag{21}$$

and the 6D mean hydrostatic stress and strain components are given by

$$\vec{\sigma}_{hm} = \sigma_{hm}\cdot\begin{bmatrix}1&1&1&0&0&0\end{bmatrix}^T \quad \text{and} \quad \vec{\varepsilon}_{hm} = \varepsilon_{hm}\cdot\begin{bmatrix}1&1&1&0&0&0\end{bmatrix}^T. \tag{22}$$

Similarly to the 2D version of the MOI method, if the PMOI I_p is integrated along a *full* loading cycle, then the path-equivalent stress or strain range also becomes

$$\Delta\sigma_{\text{Mises}} \text{ or } \Delta\varepsilon_{\text{Mises}}\cdot(1+\bar{\nu}) = \sqrt{12\cdot I_p}. \tag{23}$$

Since the norm $\left|\vec{s}'-\vec{s}'_m\right|$ is equal to the relative von Mises stress between each point $\vec{s}'$ from the path and the path centroid $\vec{s}'_m$, it is possible to interpret the MOI method for stress ranges as a root mean square (RMS) of the relative von Mises stresses along the stress path with respect to its centroid. Analogously, the MOI method for strain ranges can be interpreted as a RMS of the relative von Mises strains $\left|\vec{e}'-\vec{e}'_m\right|$ along the strain path with respect to its centroid.

This generalized MOI approach can be used in polygonal multiaxial history paths, which are useful for computational calculations with discrete finite load increments. For a deviatoric stress path defined by polygon vertices $\vec{s}'_i$, if each side i of the polygon has length equal to a finite stress increment $\left|\Delta\vec{s}'_i\right|$ and is centered at the point $\Delta\vec{s}'_i + 0.5\cdot\Delta\vec{s}'_i$, then the MOI expressions for a *full* loading cycle are obtained from a generalized version of Eq. (15):

$$\begin{aligned} p_s &= \sum_i |\Delta\vec{s}'_i|, \quad \vec{s}'_m = (1/p_s)\cdot\sum_i(\vec{s}'_i + 0.5\cdot\Delta\vec{s}'_i)\cdot|\Delta\vec{s}'_i|,\\ I_p &= (1/p_s)\cdot\sum_i\left[|\Delta\vec{s}'_i|^2/12 + |\vec{s}'_i + 0.5\cdot\Delta\vec{s}'_i - \vec{s}'_m|^2\right]\cdot|\Delta\vec{s}'_i|. \end{aligned} \tag{24}$$

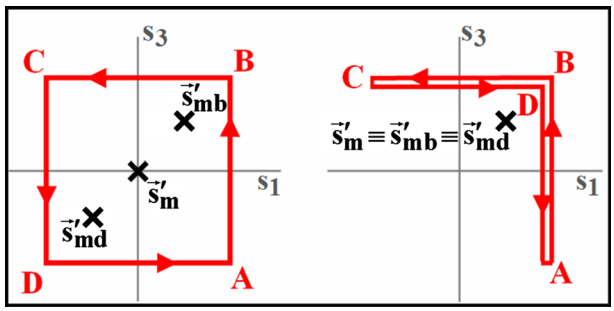

Fig. 5 Square (*left*) and *L*-shaped (*right*) deviatoric stress paths for a full cycle

Analogously, for a deviatoric strain path defined by a polygon with vertices $\vec{e}'_i$ and side lengths equal to finite strain increments $|\Delta\vec{e}'_i|$ centered at the points $\Delta\vec{e}'_i + 0.5 \cdot \Delta\vec{e}'_i$, the MOI expressions for a *full* loading cycle become

$$\begin{aligned} p_e &= \sum_i |\Delta\vec{e}'_i|, \quad \vec{e}'_m = (1/p_e) \cdot \sum_i (\vec{e}'_i + 0.5 \cdot \Delta\vec{e}'_i) \cdot |\Delta\vec{e}'_i|, \\ I_p &= (1/p_e) \cdot \sum_i \left[|\Delta\vec{e}'_i|^2/12 + |\vec{e}'_i + 0.5 \cdot \Delta\vec{e}'_i - \vec{e}'_m|^2 \right] \cdot |\Delta\vec{e}'_i|. \end{aligned} \tag{25}$$

The path-equivalent von Mises ranges $\Delta\sigma_{\text{Mises}}$ or $\Delta\varepsilon_{\text{Mises}}(1+\bar{\nu})$ for each full load cycle are then calculated from Eq. (23). For 2D paths, this generalized MOI approach gives the same path-equivalent alternate components as the 2D MOI method presented in the previous section, as expected.

To account for fatigue damage induced by complex NP multiaxial load histories with varying amplitude, where full load cycles cannot be easily identified, or by histories composed by sequences of multiple half-cycles with varying amplitudes mixed together, it is necessary to use a multiaxial rainflow-like algorithm [22,23], which must be applied before evaluating the path-equivalent stresses and strains. Note, however, that the MOI method has been defined for full cycles, whereas rainflow counts return half-cycles. So the MOI method needs to be adapted to address half-cycles, as discussed next.

The main issue here is that the mean components (i.e., the centroids) $\vec{s}'_m$ or $\vec{e}'_m$ of a full cycle might be different from the centroids of each half-cycle. For instance, consider the two deviatoric stress paths *A–B–C–D–A* shown in Fig. 5, describing a square and an *L*-shape load with sides $2a$ in an $s_1 \times s_3$ diagram. If a multiaxial rainflow count is applied to such paths starting at point *A*, two half-cycles are obtained in each case, namely *A–B–C* and *C–D–A*. In both cases, from Eq. (24), the mean component $\vec{s}'_{mb}$ of each *A–B–C* path is located at the upper *L*-shape centroid $\vec{s}'_{mb} = [\,a/2\ 0\ a/2\ 0\ 0\,]^T$ (when represented in the 5D E_{5s} space), making the PMOI $I_p \cong 0.83 \cdot a^2$ and generating the path-equivalent range $\Delta\sigma_{\text{Mises}} = 3.16 \cdot a$. The very same $\Delta\sigma_{\text{Mises}} = 3.16 \cdot a$ is found in both path examples for the other half-cycle *C–D–A*, where $\vec{s}'_{md}$ represents the centroid of this lower *L*-shape path segment, see Fig. 5.

However, when the PMOI is calculated over the *full* cycle *A–B–C–D–A*, a larger value $I_p \cong 1.33 \cdot a^2$ is found, and thus $\Delta\sigma_{\text{Mises}} = 4 \cdot a$ for the square path due to its mean component $\vec{s}'_m$ at the diagram origin, while the lower $\Delta\sigma_{\text{Mises}} = 3.16 \cdot a$ only remains valid for the *L*-shaped path. Therefore, considering the square path as two separate half-cycles would underestimate its path-equivalent range by more than 20 %, a significantly non-conservative error that cannot be tolerated in practical applications.

One solution to this issue is to consider the mean component of a *full* cycle $\vec{s}'_m$ (or $\vec{e}'_m$ for strain paths) in the calculation of the I_p integral, instead of the mean component of the half-cycle ($\vec{s}'_{mb}$ and $\vec{s}'_{md}$ in the above example). Therefore, Eq. (19) should be integrated along each full cycle (with perimeters p_s or p_e), instead of each half-cycle, from which the PMOI I_p and the path-equivalent ranges would be calculated using Eqs. (18) and (23).

However, rainflow-counted half-cycles do not usually pair up in cycles, especially in multiaxial NP histories. If a full cycle cannot be identified, then the mean components $\vec{s}'_m$ and $\vec{e}'_m$ should be calculated along a single block of a periodic portion of the load history, or along the entire history if no periodic cycles or blocks can be identified. Unfortunately, this heuristic approach is inherent to any path-equivalent stress or strain method, since it is impossible to calculate on the fly the ranges and means of a half-cycle such as *A–B–C* without considering the shape of the entire cycle *A–B–C–D–A* that will only be fully defined in the following half-cycles. However, fortunately, this approximation leads to conservative predictions, since load ranges calculated using the recommended $\vec{s}'_m$ or $\vec{e}'_m$ of the full-cycle centroid are always greater than or equal to the

ones obtained using mean values at the half-cycle centroid, such as $\vec{s}'_{mb}$ or $\vec{s}'_{md}$ in Fig. 5. The proof for this statement follows from the fact that moments of inertia achieve their minimum values at the centroid: The PMOI of a half-cycle path is minimized at the half-cycle centroid, and thus the calculation at the (better) full-cycle centroid would give a higher (more conservative) PMOI. These ideas are compared with concurrent minimum ball and maximum prismatic convex enclosure predictions for the damage induced by several load paths next.

4 Comparisons among the equivalent range prediction methods

MOI estimates of path-equivalent ranges are now compared with experimental results and with convex enclosure predictions using thirteen tension–torsion periodic histories studied by Itoh et al. [24,25], shown in the $e_1 \times e_3 = [\varepsilon_x \cdot (1+\bar{\nu}) \times \gamma_{xy}\sqrt{3}/2]$ strain-controlled paths from Fig. 6 for Cases 0 through 12.

Although these 13 tests are all 2D, they are the best experimental results available in the literature and as so can be used to compare the MOI with the other estimations methods. Fully 6D histories have not been found, even because there is no commercial equipment available to apply and control them. Nevertheless, those 2D multiaxial load histories can identify the shortcomings of equivalent range predictions, so they are appropriate to evaluate them, as well as to confirm that the presented 6D formulation exactly reproduces the original 2D MOI method for 2D tension–torsion histories.

For large plastic strains, where the effective Poisson ratio $\bar{\nu} \cong 0.5$, this deviatoric strain diagram can be approximated by the normal-shear diagram given by $e_1 \times e_3 \cong [\varepsilon_x \cdot 1.5 \times \gamma_{xy}\sqrt{3}/2] = 1.5 \cdot (\varepsilon_x \times \gamma_{xy}/\sqrt{3})$, which is usually scaled down in the literature to the equivalent $\varepsilon_x \times \gamma_{xy}/\sqrt{3}$ diagram.

Note that each block of the periodic paths from Fig. 6 is usually associated with one cycle, except for Cases 1–4, which contain two cycles per block. The number of cycles associated with any stress or strain path can be deterministically calculated using a multiaxial rainflow algorithm, such as the ones presented in [22,23].

Table 1 shows the predicted ratios $\lambda = \Delta\varepsilon_{\text{Mises}}(1+\bar{\nu})/L$ between the path-equivalent strain ranges and the longest chord L of the path, according to the MOI, minimum ball (MB) [10], and Maximum Prismatic Hull (MPH) [8] methods, compared to experimental measurements from [24,25] in a 304 stainless steel. These ratios are calculated from Itoh's experimental strain paths using Eq. (25) and then (23) for the MOI, and finding the minimum ball and maximum rectangle that enclose such paths for the MB and MPH methods, as described in [1].

This material is appropriate to identify the differences between the various equivalent range estimation methods because it is particularly sensitive to non-proportional multiaxial loads (those that induce varying principal stress directions, thus different fatigue damage in different planes that pass through the critical point, as discussed in [2]). The conclusions from these MOI and convex enclosure prediction comparisons are:

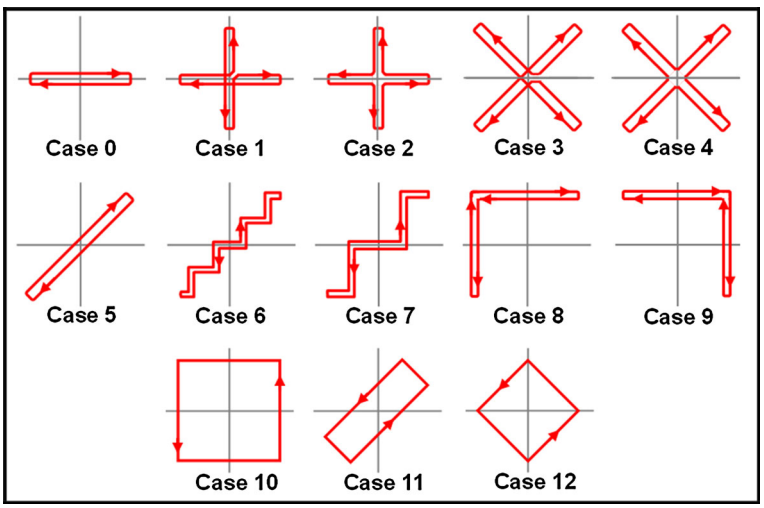

Fig. 6 Strain-controlled tension–torsion paths $e_1 \times e_3 = [\varepsilon_x \cdot (1+\bar{\nu}) \times \gamma_{xy}\sqrt{3}/2]$ used in the experimental validation of the MOI method to predict path-equivalent ranges

Table 1 Predictions of the ratios $\lambda = \Delta\varepsilon_{\text{Mises}}(1+\bar{\nu})/L$ between the path-equivalent strain ranges and the longest chord L of the applied deviatoric strain path according to the MOI, MB, and MPH methods for the 13 tension–torsion cases, calculated from Itoh's data

path / λ	MOI	MB	MPH
Case 0	1	1	1
Case 1	1*	1	√2
Case 2	1*	1	√2
Case 3	1*	1	√2
Case 4	1*	1	√2
Case 5	1	1	1
Case 6	1.01	1	1.03
Case 7	1.03	1	1.06
Case 8	1.12	1	1.14
Case 9	1.12	1	1.14
Case 10	√2	1	√2
Case 11	1.263	1	1.263
Case 12	1.411	1	1.411

as if 90° out of phase

good predictions

good predictions

as if proportional

1. The MB method [10] is not able to identify the significant non-proportionality of Cases 8–12, wrongfully returning the same equivalent ranges as the proportional paths from Cases 0 and 5, as verified in Table 1.
2. The MPH [8] (and its variations, as well as the Minimum F-norm Ellipsoid [7]) is efficient to predict equivalent ranges in simple NP histories; however, it does not perform well in cross or star-shaped paths such as the ones from Cases 1–4, wrongfully returning the same ranges as the highly NP Case 10. For a general NP loading, it is difficult to justify that a convex enclosure that does not represent well the shape or even the mean component of a path can be used to calculate its path-equivalent ranges or amplitudes. This is even more difficult to justify when the stress or strain path is not convex or has a very odd shape in such deviatoric diagrams.
3. The MOI method, on the other hand, can estimate both path-equivalent ranges and mean components with a much better coherence than any convex enclosure method. Moreover, since it accounts for the contribution of every single segment of the path, the MOI method can deal with arbitrarily shaped non-convex histories without losing information about such shapes, as the convex enclosure methods would.

Therefore, the MOI method can be successfully used even in highly non-convex stress or strain NP load history paths such as the cross or star-shaped Cases 1–4. So, it is recommended to better predict multiaxial fatigue lives, as seen in Fig. 7 for the data from [24,25] measured in 304 stainless steel tension–torsion specimens subjected to the thirteen strain histories used in this comparison. Note that all multiaxial fatigue life predictions shown in Fig. 7 are based on the critical plane approach [14,15] using the multiaxial version of the Smith–Watson–Topper (SWT) damage model [26], usually called the SWT-Bannantine approach.

Note in Fig. 7 the five too non-conservative MB predictions for Cases 8–12, and the four too conservative MPH predictions for Cases 1–4, while the MOI multiaxial fatigue life predictions fall within 20 % of the experimental values for all thirteen tension–torsion histories.

In summary, the MOI method is relatively simple, intuitive, and easy to implement and to compute numerically. It is thus a better practical alternative to convex enclosure methods to estimate path-equivalent amplitude/range and mean components of multiaxial NP load histories, with a low computational cost and without the need for adjustable coefficients.

In fact, coupled with an efficient multiaxial rainflow algorithm, it has been implemented in the *ViDa 3D* software [27] to deal with very long 6D NP variable amplitude histories in practical applications. Moreover, when computed in a deviatoric plastic strain space, the MOI method is also able to predict non-proportionality

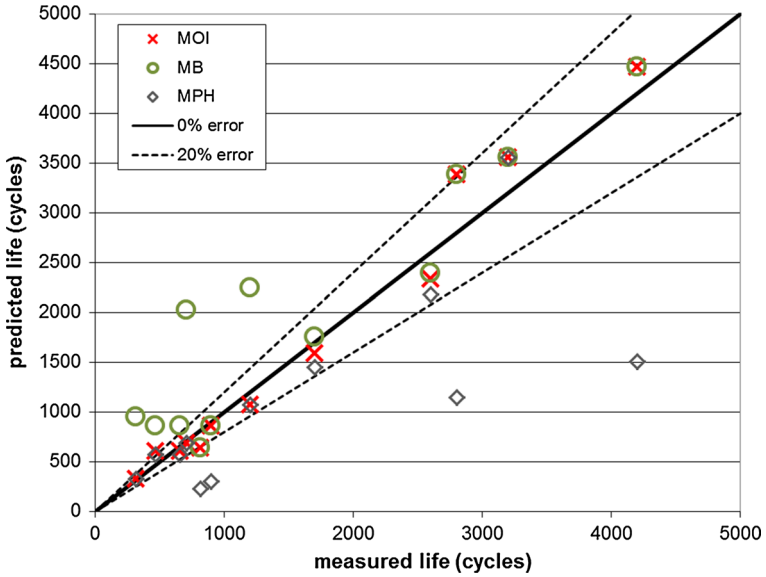

Fig. 7 Measured and predicted fatigue lives for the 13 tension–torsion strain-controlled load cases using the MOI, MB, and MPH methods, for a 304 stainless steel

factors of NP load histories [28], which are important to predict additional hardening effects under NP loading observed in materials with low stacking fault energy such as austenitic stainless steels.

5 Conclusions

In this work, the MOI method has been generalized to 6D non-proportional multiaxial load histories, to calculate their equivalent amplitude/range and mean components. It accounts for the contribution of every single segment of the stress or strain path, dealing with an arbitrarily shaped history without losing information about the shape, so it is a better option to find equivalent ranges than the concurrent convex enclosure methods. Experimental results demonstrated its effectiveness to predict ranges and associated multiaxial fatigue lives for a 304 stainless steel alloy. Further experiments on different materials should be conducted to verify the applicability of the MOI method to, e.g., low-alloy steels and aluminum alloys.

Acknowledgments The authors would like to acknowledge Prof. Darrell F. Socie for providing the experimental data used in the analyses. This work was supported in part by the National Natural Science Foundation of P.R. China under Grant No. 11302150. CNPq-Brazil provided research fellowships for Profs. Marco A. Meggiolaro and Jaime T.P. Castro.

References

1. Meggiolaro, M.A., Castro, J.T.P.: An improved multiaxial rainflow algorithm for non-proportional stress or strain histories—part I: enclosing surface methods. Int. J. Fatigue **42**, 217–226 (2012)
2. Socie, D.F., Marquis, G.B.: Multiaxial Fatigue. Society of Automotive Engineers, Inc., Warrendale (2000)
3. Freitas, M., Li, B., Santos, J.L.T.: A numerical approach for high-cycle fatigue life prediction with multiaxial loading. In: Multiaxial Fatigue and Deformation: Testing and Prediction, ASTM STP 1387, ASTM (2000)
4. Li, B., Santos, J.L.T., Freitas, M.: A unified numerical approach for multiaxial fatigue limit evaluation. Mech. Struct. Mach. **28**(1), 85–103 (2000)
5. Li, B., Santos, J.L.T., Freitas, M.: A computerized procedure for long-life fatigue assessment under multiaxial loading. Fatigue Fract. Eng. Mater. Struct. **24**, 165–177 (2001)
6. Gonçalves, C.A., Araújo, J.A., Mamiya, E.N.: Multiaxial fatigue: a stress based criterion for hard metals. Int. J. Fatigue **27**, 177–187 (2005)
7. Zouain, N., Mamiya, E.N., Comes, F.: Using enclosing ellipsoids in multiaxial fatigue strength criteria. Eur. J. Mech. A Solids **25**, 51–71 (2006)
8. Mamiya, E.N., Araújo, J.A., Castro, F.C.: Prismatic hull: a new measure of shear stress amplitude in multiaxial high cycle fatigue. Int. J. Fatigue **31**, 1144–1153 (2009)
9. Deperrois, A.: Sur le calcul des limites d'endurance des aciers. Ph.D. Thesis, Ecole Poly-technique, Paris (1991)

10. Ballard, P., Dang Van, K., Deperrois, A., Papadopoulos, I.V.: High cycle fatigue and a finite element analysis. Fatigue Fract. Eng. Mater. Struct. **18**(3), 397–411 (1995)
11. Araújo, J.A., Dantas, A.P., Castro, F.C., Mamiya, E.N., Ferreira, J.L.A.: On the characterization of the critical plane with a simple and fast alternative measure of the shear stress amplitude in multiaxial fatigue. Int. J. Fatigue **33**(8), 1092–1100 (2011)
12. Castro, F.C., Araújo, J.A., Mamiya, E.N., Zouain, N.: Remarks on multiaxial fatigue limit criteria based on prismatic hulls and ellipsoids. Int. J. Fatigue **31**(11), 1875–1881 (2009)
13. Kane, T.R., Levinson, D.A.: Dynamics, Theory and Applications. McGraw-Hill, New York (2005)
14. Bannantine, J.A.: A Variable Amplitude Multiaxial Fatigue Life Prediction Method. FCP Report n. 151, University of Illinois at Urbana-Champaign (1989)
15. Bannantine, J.A., Socie, D.F.: A variable amplitude multiaxial fatigue life prediction method. In: Fatigue Under Biaxial and Multiaxial Loading, vol. 10, pp. 35–51. ESIS (1991)
16. Sines, G.: Behavior of metals under complex static and alternating stresses. In: Metal Fatigue, pp. 145–169. McGraw-Hill (1959)
17. Crossland, B.: Effect of large hydrostatic pressures on the torsional fatigue strength of an alloy steel. In: International Conference on Fatigue of Metals, pp. 138–149. IMechE, London (1956)
18. Papadopoulos, I.V.: A new criterion of fatigue strength for out-of-phase bending and torsion of hard metals. Int. J. Fatigue **16**, 377–384 (1994)
19. Papuga, J., Ruzicka, M.: Two new multiaxial criteria for high cycle fatigue computation. Int. J. Fatigue **30**, 58–66 (2008)
20. Novozhilov, V.V.: Theory of Elasticity (J. J. Sherrkon trans.), Jerusalem: Israel Program for Scientific Translation (1961)
21. Mandel, J.: Cours de Mécanique des Milieux Continus, tomes I and II. Gauthier-Villars, Paris (1966)
22. Wang, C.H., Brown, M.W.: Life prediction techniques for variable amplitude multiaxial fatigue—part 1: theories. J. Eng. Mater. Technol. **118**, 367–370 (1996)
23. Meggiolaro, M.A., Castro, J.T.P.: An improved multiaxial rainflow algorithm for non-proportional stress or strain histories—part II: the modified Wang–Brown method. Int. J. Fatigue **42**, 194–206 (2012)
24. Itoh, T., Sakane, M., Ohnami, M., Socie, D.F.: Nonproportional low cycle fatigue criterion for type 304 stainless steel. ASME J. Eng. Mater. Technol. **117**, 285–292 (1995)
25. Itoh, T., Chen, X., Nakagawa, T., Sakane, M.: A simple model for stable cyclic stress–strain relationship of type 304 stainless steel under nonproportional loading. J. Eng. Mater. Technol. **122**, 1–9 (1995)
26. Smith, R.N., Watson, P., Topper, T.H.: A stress–strain parameter for the fatigue of metals. J. Mater. **5**(4), 767–778 (1970)
27. Meggiolaro, M.A., Castro, J.T.P.: Automation of the fatigue design under variable amplitude loading using the ViDa software. Int. J. Struct. Integr. **1**, 1–6 (2010)
28. Meggiolaro, M.A., Castro, J.T.P.: Prediction of non-proportionality factors of multiaxial histories using the moment of inertia method. Int. J. Fatigue **61**, 151–159 (2014)